RSC Advances

ROYAL SOCIETY OF CHEMISTRY

www.rsc.org/advances

RSC Advances

COMMUNICATION

SDBS-assisted hydrothermal synthesis of flower-like Ni-Mo-S catalysts and their enhanced hydrodeoxygenation activity

Weiyan Wang,*[a,b] Song Tan,[a] Guohua Zhu,[a] Kui Wu,[a] Liang Tan,[a] Yingze Li,[a] Yunquan Yang*[a,b]

Received 00th January 20xx,
Accepted 00th January 20xx

DOI: 10.1039/x0xx00000x

www.rsc.org/

Ni-Mo-S catalsyts were prepared by sodium dodecyl benzene sulfonate (SDBS) assisted hydrothermal synthesis. The presence of SDBS increased the NiS_2 crystallite size, enlarged the interlayer distance of MoS_2 plane and formed loose flower-like architecture, which contributed to the enhanced HDO activity. Comparerd with Ni-Mo-S synthesized at the absence of SDBS, *p*-cresol conversion, methylcyclohexane selectivity and deoxygenation degree was increased by 24%, 25.1% and 26.3%, respectively.

Due to the increasing energy consumption and environmental pollution, bio-oil, derived from the fast pyrolysis of biomass, has been considered as a sustainable, renewable and clean replacement material for the production of fuel and chemicals and consequently attracted much attention.[1, 2] Unfortunately, this bio-oil contained high oxygen content, leading to some deleterious properties, e.g., a low heating value, which could not be utilized directly as a supplementary for transportation fuel. Aiming to decrease the oxygen content, catalytic hydrodeoxygenation (HDO) was an interesting and effective technology for the selective removal of oxygen atom from bio-oil at the presence of hydrogen and a moderate reaction temperature.[3] Since phenols were the major monomers for the lignin fraction of biomass and the scission of $C_{aromatic}$–OH bond was harder than other C–O bonds,[4] they were usually used as model compounds to evaluate the HDO activity of the prepared catalysts.

Up to now, the catalysts for the HDO of phenols included amorphous metal borides,[5-7] metal catalyst,[8-10] noble metal catalysts,[11-14] transition metal phosphide,[15-17] carbide,[18] oxide[19] and sulfide catalysts.[20-22] However, the low thermal stability, high cost or low HDO activity of prevented some of these catalysts from industrial commercialization. Mo based sulfides, a kind of commercial catalysts for hydrodesulfurization reactions, had been extensively applied into the HDO reactions,[2] but their morphologies depended on the synthesis methods and played an important role in the catalytic activity and product distribution.[23] Customarily, traditional sulfides were prepared by sulfurization with toxic gas H_2S, and their activities was closely related to the sulfurization conditions.[24] Moreover, this process required high temperature to obtain the desired phases and resulted in an ordered crystalline MoS_2 with large particle size. It had confirmed that amorphous structure supplied more available unsaturated active sites for reactions and then enhanced the catalytic activity.[25, 26] For example, B Yoosuk et al.[27] had prepared amorphous unsupported Ni–Mo bimetal sulfides with high surface area by one step hydrothermal method and concluded their high HDO activities.

Adding surfactant as a soft template during the synthesis of Mo based sulfides was a normal strategy to control their morphologies.[28] C. Li et al.[29] had reported that Pluronic F-127 had a significant effect on the formation of flower-like MoS_2. S. Miao et al.[30] had found that tetraethylorthosilicate was crucial to form exfoliated MoS_2 with ultra-small sheets and high specific surface area (101.6 m^2/g). Y. Tang et al.[31] had demonstrated that PVP-assisted synthesis was an efficient and scalable method for the preparation of MoS_2 nanosheets. L. Ma et al.[32] had prepared few-layer and edge-rich MoS_2 nanospheres by adding SDBS. However, although previous studies had shown the high activity of Ni–Mo bimetal sulfide in the HDO of phenols,[27, 33] these catalysts were not prepared by SDBS-assisted hydrothermal synthesis before. Therefore, in this communication, the effects of SDBS addition amount on the structures and HDO activities of Ni-Mo-S catalsyts were studied.

Fig. 1 showed the XRD patterns of Ni-Mo bimetal sulfide catalysts prepared by adding different amount of SDBS. Without adding SDBS, the peak at 2θ=14° in the XRD pattern of Ni-Mo-S was attributed to the typical (002) plane of MoS_2,[34, 35] while the peaks at 2θ=32°, 36°, 54° and 57° to cubic phase NiS_2[36] and 2θ= 45° to the characteristic of amorphous structure.[37, 38] Compared with crystalline MoS_2 in the previous studies,[35, 39] all peaks at 2θ= 33°, 39°and 59° became much weaker, indicating that Ni-Mo-S had a poorly crystallization and MoS_2 and NiS_2 were uniformly dispersed in the resultant catalysts. At the presence of SDBS, some new peaks were observed at 2θ=27°, 32°, 36°, 39°, 45° and 53°, attributing to cubic NiS_2,[36] which became

[a] School of Chemical Engineering, Xiangtan University, Xiangtan City, Hunan 411105, P R China
E-mail: wangweiyan@xtu.edu.cn, yangyunquan@xtu.edu.cn.
[b] National & Local United Engineering Research Center for Chemical Process Simulation and Intensification, Xiangtan University, Xiangtan 411105, P. R. China
† Electronic Supplementary Information (ESI) available: See
DOI: 10.1039/x0xx00000x

obvious and sharp, especially for Ni-Mo-S-0.3. These suggested that the addition of SDBS had a great effect on NiS_2 crystallite size in Ni-Mo-S catalysts.

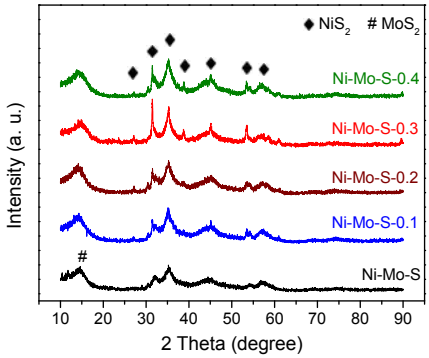

Fig. 1 XRD patterns of the as-prepared Ni-Mo bimetal sulfide catalysts

According to the XRD results, the NiS_2 crystallite size was calculated by the Scherrer formula: $D = K\lambda/(\beta\cos\theta)$.[40] As shown in Table 1, the average crystallite size of NiS_2 in Ni-Mo-S, Ni-Mo-S-0.1, Ni-Mo-S-0.2, Ni-Mo-S-0.3 and Ni-Mo-S-0.4 was 11.8 nm, 27.5 nm, 31.5 nm, 41.2 nm and 39.7 nm, respectively, indicating that adding SDBS during the synthesis process increased the NiS_2 crystallite size. It had reported that Ni-Mo-S phase formed and possibly presented as nano-size particles in the catalysts when they were prepared by one step hydrothermal method, leading to no appearance in the XRD pattern.[41] However, in this study, the Ni/Mo molar ratio was only 0.3, but there displayed obvious NiS_2 phase in Fig. 1. Moreover, the crystallite size of NiS_2 was changed with the SDBS addition amount. These revealed that no or very small proportion of Ni-Mo-S phase formed in the resultant Ni-Mo bimetal sulfide catalysts.

Table 1 Physical properties of Ni-Mo bimetal sulfide catalysts

Catalyst	Surface area (m^2/g)	NiS_2 Crystallite size (nm)
Ni-Mo-S	7.9	11.7
Ni-Mo-S-0.1	7.2	27.5
Ni-Mo-S-0.2	5.6	31.5
Ni-Mo-S-0.3	7.5	41.2
Ni-Mo-S-0.4	9.0	39.7

The morphologies of Ni-Mo bimetal sulfide catalysts were observed using SEM and TEM, as shown in Fig. 2. Ni-Mo-S showed a hollow sphere morphology with a diameter of about 1.5 μm and wall thickness of 0.4 μm. This morphology might be formed from the self-assembly of sheet-like subunits in ordered orientation. After adding SDBS, e.g., Ni-Mo-S-0.2, the hollow sphere morphology vanished, but sphere-like particles with a diameter of about 0.6 μm appeared. Ni-Mo-S-0.3 presented a loose flower-like architecture, which was resulted from the random self-assembly of nano-sheets. According to the possible formation mechanism for Mo based sulfides in the previous literatures,[42, 43] the hollow sphere morphology was elucidated as following: (1) nucleation and growth into primary nanoparticles, (2) orientated growth into nano-sheets and (3) oriented self-assembly into hollow sphere. Compared with the different morphologies in Fig. 2, the third step that nano-sheets self-assembly was the crucial step for the final morphology. Because SDBS had an aromatic headgroup and a hydrophobic tail, it could insert in the interspace between nano-sheets and effectively inhibit the aggregation of nano-sheets. Consequently, the hollow sphere was broken, and the the nano-sheets self-assembled to form flower-like morphology. In addition, it had presumed that SDBS could produce an interaction with MoS_4^{2-} anions due to the chemical coupling effect originating from the highly delocalized π electrons of benzene ring and the external electrons of the sulfur atoms.[32] This interaction could stabilize the nano-sheets and then decreased the thickness. As shown in Fig. 2, when the SDBS amount increased from 0.2 g to 0.4 g, the nano-sheet thickness gradually reduced. Their surface areas were in line with the SEM results. As listed in table 1, because of the fill of NiS_2 in MoS_2 pores, all the surface areas were very low. Ni-Mo-S, Ni-Mo-S-0.1, Ni-Mo-S-0.2, Ni-Mo-S-0.3 and Ni-Mo-S-0.4 presented a surface area of 7.9 m^2/g, 7.2 m^2/g, 5.6 m^2/g, 7.5 m^2/g and 9.0 m^2/g, respectively. The surface area was decreased after the change of hollow sphere into the solid sphere, but which was increased when the nano-sheet thickness became thinner.

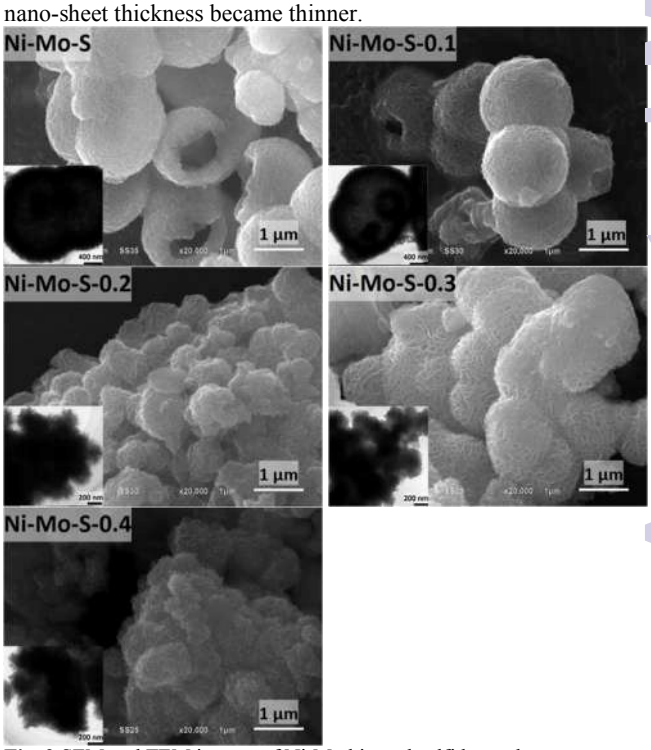

Fig. 2 SEM and TEM images of Ni-Mo bimetal sulfide catalysts

To further investigate the effect of SDBS on the microstructure of Ni-Mo bimetal sulfide catalysts, the prepared samples were characterized by HRTEM, as shown in Fig. 3. All the images presented two kinds of parallel fringes: One group with an interlayer distance of 0.65-0.72 nm and the other one with an interplanar spacing of 0.27 nm, characterizing the (002) plane of MoS_2[44, 45] and (200) plane of cubic NiS_2,[46, 47] respectively. These also suggested that Ni and Mo were existed in the separated sulfide phases in Ni-Mo bimetal sulfide catalysts. Interestingly, with the increment of SDBS amount, the interlayer distance for (002) plane of MoS_2 was enlarged, which was caused by the aromaticity of the headgroup in SDBS. At the presence of SDBS, it acted as an exfoliator and inserted into the interlayer of nano-sheets to disrupt the van der Waals interaction between MoS_2 layers.[48, 49] This enlarged interlayer distance was expected to be favorable for the co-planar absorption of phenols via the aromatic ring and exhibited high hydrogenation selectivity.

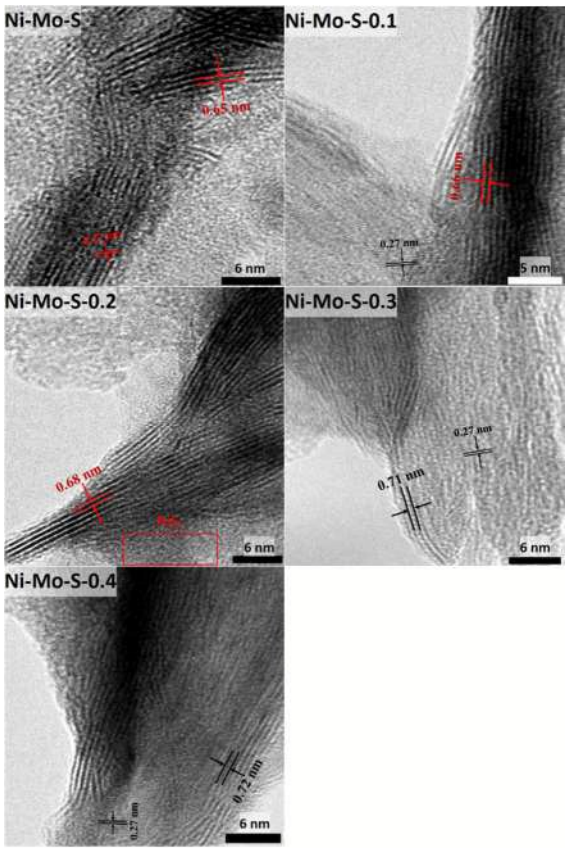

Fig. 3 TEM images of Ni-Mo bimetal sulfide catalysts

The catalytic activity of the prepared Ni-Mo bimetal sulfide catalysts were tested taking the HDO of *p*-cresol as a probe. The concentration changes of reactant and products versus reaction time on Ni-Mo-S and Ni-Mo-S-0.3 are shown in Fig. 4. Previously, two reaction routes had been proposed in the HDO of phenols based on the product distributions: (i) direct deoxygenation (DDO) via C–O bond scission and (ii) hydrogenation–deoxygenation (HYD) via saturation of the aromatic ring followed by the dehydration. Fig. 4 (a) showed that the main products in the HDO of *p*-cresol on Ni-Mo-S were toluene, methylcyclohexane and 3-methylcyclohexene, and not any oxygen-containing compound was detected during the whole reaction, suggesting that the hydrogenation of the aromatic ring was the limited step for HYD route. The increasing toluene and methylcyclohexane concentrations with the reaction time indicated that DDO and HYD routes were simultaneously occured, where toluene was the product of DDO route while methylcyclohexane and 3-methylcyclohexene produced from the HYD route. According to these product concentrations, it could be concluded that DDO route was superior to HYD route on Ni-Mo-S catalyst. However, previous studies[27, 50, 51] had reported that the addition of promoter Ni into MoS_2 enhanced the hydrogenation activity and made HYD to be the main HDO route for phenols. This change on the HDO reaction route was resulted from the different synthesis method of the catalyst. For example, D. Wang et al.[52] had reported that toluene selectivity was higher than 90% on Ni-Mo-W sulfide catalyst prepared by mechanical activation method. In contrast, although the HDO of *p*-cresol on Ni-Mo-S-0.3 presented the same products as that on Ni-Mo-S, their contents varied greatly. The product concentration at the same reaction time decreased in the order of methylcyclohexane > toluene > 3-methylcyclohexene, indicating that the main HDO route changed toward to HYD. These demonstrated that adding SDBS into the synthesis of Ni-Mo bimetal sulfide enhanced the hydrogenation activity.

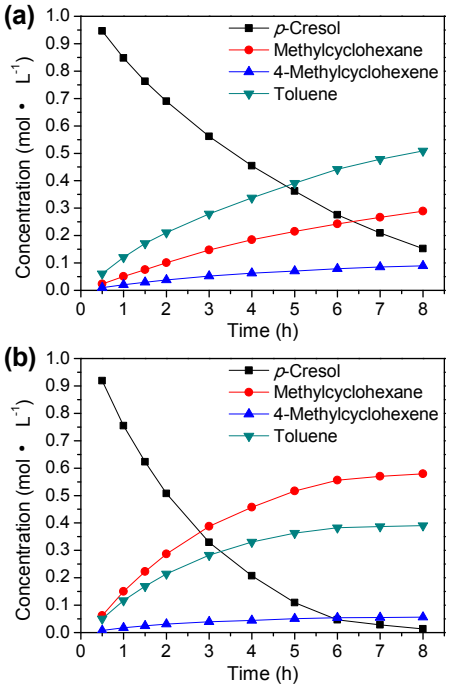

Fig. 4 Concentration changes of reactant and products versus reaction time in the HDO of *p*-cresol on (a) Ni-Mo-S and (b) Ni-Mo-S-0.3

Table 2 The HDO of *p*-cresol on Ni-Mo-S, Ni-Mo-S-0.1, Ni-Mo-S-0.2, Ni-Mo-S-0.3 and Ni-Mo-S-0.4 at 275 °C for 6 h

Catalyst	Ni-Mo-S	Ni-Mo-S-0.1	Ni-Mo-S-0.2	Ni-Mo-S-0.3	Ni-Mo-S-0.4
Conversion (mol %)	71.5	82.8	85.8	95.5	92.6
$k\times10^2$, mL/(s·g catalyst)	2.4	3.3	3.4	4.6	3.7
Products selectivity (mol %)					
Methylcyclohexane	30.8	33.7	49.1	56.0	59.3
3-Methylcyclohexene	10.4	9.3	4.8	5.5	6.7
Toluene	58.8	57.0	46.1	38.5	34.0
H/C molar ratio	1.47	1.48	1.59	1.65	1.69
D. D. (wt %)	68.6	80.8	84.2	94.9	87.3

RSC Advances

COMMUNICATION

The comparison of Ni-Mo-S, Ni-Mo-S-0.1, Ni-Mo-S-0.2, Ni-Mo-S-0.3 and Ni-Mo-S-0.4 on the HDO activity are shown in Table 2. According to the previous conclusions,[53, 54] the decomposition of *p*-cresol was modeled to be a pseudo-first-order reaction and the reaction rate constant *k* (*mL/(s·g catalyst)*) was calculated according to the equation $\ln(1-x)=-k\cdot C_{cat}\cdot t$. After reaction at 275 °C for 6 h, *p*-cresol conversion on Ni-Mo-S was 71.5% with a selectivity of 30.8% methylcyclohexane and a deoxygenation degree of 68.6%. With the increment of SDBS, *p*-cresol conversion increased first and then decreased while methylcyclohexane selectivity increased gradually. The corresponding *k* at 275 °C increased with the order of Ni-Mo-S (2.4×10^{-2}) < Ni-Mo-S-0.1 (3.3×10^{-2}) < Ni-Mo-S-0.2 (3.4×10^{-2}) < Ni-Mo-S-0.4 (3.7×10^{-2}) < Ni-Mo-S-0.3 (4.6×10^{-2}), showing the highest HDO activty of Ni-Mo-S-0.3. It had reported that the highest reaction rate constant *k* on Ni-Mo bimetal sulfides prepared without adding SDBS was 3.2×10^{-2} mL/(s·g catalyst) at 300 °C,[33] which was much lower than that in this study because the *k* increased with the raising of reaction temperature.[55] Compared with Ni-Mo-S, *p*-cresol conversion, methylcyclohexane selectivity and deoxygenation degree on Ni-Mo-S-0.3 was increased by 24%, 25.1% and 26.3% under the same reaction conditions, respectively. But further increasing SDBS amount would reduce the HDO activity, e.g., 87.3% deoxygenation degree on Ni-Mo-S-0.4. Hence, adding an appropriate SDBS in the synthesis of Ni-Mo bimetal sulfide could maximize its HDO activity.

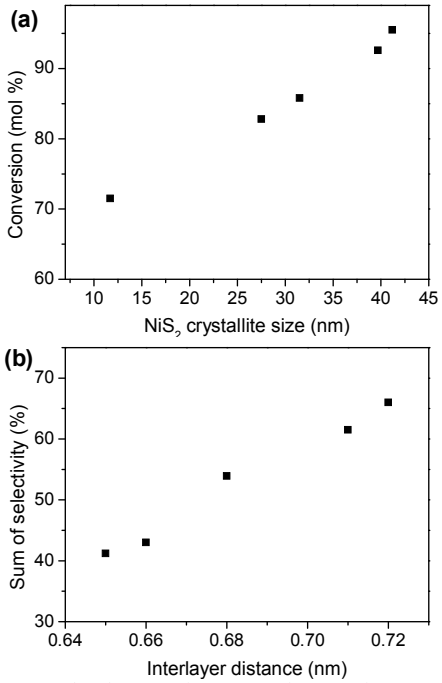

Fig. 5 The changes of (a) p-cresol conversion versus Ni_2S crystallite size and (b) the sum of selectivity of methylcyclohexane and methylcyclohexene versus interlayer distance between MoS_2 (002) plane

For the HDO of *p*-cresol, the different absorption ways decided the reaction routes.[56, 57] Vertical orientation absorption facilitated the direct C–O bond scission to form toluene while coplanar adsorption caused to the saturation of aromatic ring first and then deoxygenated to yield methylcyclohexane as the final product. The XRD and TEM results indicated that no or very little of Ni-Mo-S phase but seperated Ni and Mo sulfides phases presented in the resultant catalysts, hence the HDO reaction mechanism could be explained by the control remote model. Spillover hydrogen generated on the donor phase (Ni[illegible]) and then migrated onto the acceptor phase (MoS_2) for the HDO reaction after *p*-cresol was absorbed on MoS_2.[58] The positive effect of adding SDBS in the synthesis of Ni-Mo bimetal sulfide catalyst on the HDO activity might be related to following factors. Firstly, as shown in Fig. 5 (a), *p*-cresol conversion increased with NiS_2 average crystallite size. Ni-Mo-S-0.3 had the largest NiS_2 crystallite size (41.2 nm) and exhibited the highest conversion (95.5%). The larger the NiS_2 crystallite size was, the more hydrogen supplied on NiS_2, and the higher was the conversion. Secondly, Fig. 3 and Table 2 displayed that the interlayer distance for (002) plane of MoS_2 and H/C molar ratio increased with the SDBS amount. This suggested that higher interlayer promoted the coplanar adsorption and then raised the hydrogenation products selectivity. As shown in Fig. 5 (b), the sum selectivity of methylcyclohexane and methylcyclohexene on Ni-Mo-S-0.4 was the largest. Last but not least, Ni-Mo-S-0.3 presented a loose flower-like structure. Compared with the hollow spheres that had most of the surface area inside and not as accessible to *p*-cresol molecules, this special structure could provide more void space for the transfer of substrate and product molecules and more active sites for reactions,[45] which enhanced the HDO catalytic activity.

Conclusions

Ni-Mo-S catalsyts were prepared by SDBS-assisted hydrothermal synthesis and the effect of SDBS addition amount during the synthesis on their structures and HDO activities were studied. The presence of SDBS increased the NiS_2 crystallite size and changed the morphnology of the catalyst. The interlayer distance for (002) plane of MoS_2 increased with SDBS addition amount. In the HDO of *p*-cresol, adding an appropriate SDBS in the catalyst synthesis could obtain Ni-Mo bimetal sulfide with a maximum HDO activity, which was resulted from the larger NiS_2 crystallite size, the increased interlayer distance for (002) plane of MoS_2 and its flower-like morphology. The pseudo-first-order reaction rate constant *k* reached to 4.6×10^{-2} mL/(s·g catalyst) at 275 °C and the deoxygenation degree raise to 96.9% for 6 h.

Acknowledgements

This research was supported by the National Natural Science Foundation of China (No. 21306159, 21376202), Scientific Research Fund of Hunan Provincial Education Department (15B234) and Students' Innovation and Entrepreneurship Training Program of Hunan Province (2015xtusj011).

Notes and references

1. C. Liu, H. Wang, A. M. Karim, J. Sun and Y. Wang, *Chem. Soc. Rev.* , 2014, **43**, 7594-7623.
2. M. Saidi, F. Samimi, D. Karimipourfard, T. Nimmanwudipong, B. C. Gates and M. R. Rahimpour, *Energy Environ. Sci.* , 2014, **7**, 103-129.
3. J. Zakzeski, P. C. A. Bruijnincx, A. L. Jongerius and B. M. Weckhuysen, *Chem. Rev.* , 2010, **110**, 3552-3599.
4. H. Wang, J. Male and Y. Wang, *ACS Catal.*, 2013, **3**, 1047-1070.
5. W. Wang, P. Liu, K. Wu, K. Zhang, L. Li, Z. Qiao and Y. Yang, *New J. Chem.* , 2015, **39**, 813-816.
6. W. Wang, Z. Qiao, K. Zhang, P. Liu, Y. Yang and K. Wu, *RSC Adv.*, 2014, **4**, 37288-37295.
7. W. Wang, Y. Yang, H. Luo, H. Peng and F. Wang, *Ind. Eng. Chem. Res.* , 2011, **50**, 10936-10942.
8. W. Song, Y. Liu, E. Barath, C. Zhao and J. A. Lercher, *Green Chem.* , 2015, **17**, 1204-1218.
9. T. Mochizuki, S.-Y. Chen, M. Toba and Y. Yoshimura, *Appl. Catal. B: Environ.*, 2014, **146**, 237-243.
10. T. M. Huynh, U. Armbruster, M.-M. Pohl, M. Schneider, J. Radnik, D.-L. Hoang, B. M. Q. Phan, D. A. Nguyen and A. Martin, *ChemCatChem* 2014, **6**, 1940-1951.
11. L. Wang, J. Zhang, X. Yi, A. Zheng, F. Deng, C. Chen, Y. Ji, F. Liu, X. Meng and F.-S. Xiao, *ACS Catal.*, 2015, **5**, 2727-2734.
12. M.-Y. Chen, Y.-B. Huang, H. Pang, X.-X. Liu and Y. Fu, *Green Chem.* , 2015, **17**, 1710-1717.
13. Y. Hong, H. Zhang, J. Sun, K. M. Ayman, A. J. R. Hensley, M. Gu, M. H. Engelhard, J.-S. McEwen and Y. Wang, *ACS Catal.*, 2014, **4**, 3335-3345.
14. C. Zhao, Y. Kou, A. A. Lemonidou, X. Li and J. A. Lercher, *Angew. Chem. Int. Ed.* , 2009, **48**, 3987-3990.
15. J.-S. Moon, E.-G. Kim and Y.-K. Lee, *J. Catal.* , 2014, **311**, 144-152.
16. W. Wang, K. Zhang, H. Liu, Z. Qiao, Y. Yang and K. Ren, *Catal. Commun.* , 2013, **41**, 41-46.
17. Y. Yang, A. Gilbert and C. Xu, *Appl. Catal. A: Gen.*, 2009, **360**, 242-249.
18. P. M. Mortensen, H. W. P. de Carvalho, J.-D. Grunwaldt, P. A. Jensen and A. D. Jensen, *J. Catal.* , 2015, **328**, 208-215.
19. M. Shetty, K. Murugappan, T. Prasomsri, W. H. Green and Y. Román-Leshkov, *J. Catal.* , 2015, **331**, 86-97.
20. S. Mukundan, M. Konarova, L. Atanda, Q. Ma and J. Beltramini, *Catal. Sci. Technol.*, 2015, **5**, 4422-4432.
21. W. Wang, K. Zhang, Z. Qiao, L. Li, P. Liu and Y. Yang, *Ind. Eng. Chem. Res.* , 2014, **53**, 10301-10309.
22. V. N. Bui, D. Laurenti, P. Afanasiev and C. Geantet, *Appl. Catal. B: Environ.*, 2011, **101**, 239-245.
23. Y. Q. Yang, C. T. Tye and K. J. Smith, *Catal. Commun.* , 2008, **9**, 1364-1368.
24. F. Niefind, W. Bensch, M. Deng, L. Kienle, J. Cruz-Reyes and J. M. Del Valle Granados, *Appl. Catal. A: Gen.*, 2015, **497**, 72-84.
25. Z. Zhu, J. Ma, L. Xu, L. Xu, H. Li and H. Li, *ACS Catal.*, 2012, **2**, 2119-2125.
26. Y. Zhu, F. Liu, W. Ding, X. Guo and Y. Chen, *Angew. Chem. Int. Ed.* , 2006, **45**, 7211-7214.
27. B. Yoosuk, D. Tumnantong and P. Prasassarakich, *Fuel*, 2012, **91**, 246-252.
28. X. Wang, Z. Zhang, Y. Chen, Y. Qu, Y. Lai and J. Li, *J. Alloys Compd.* , 2014, **600**, 84-90.
29. G. Tang, Y. Wang, W. Chen, H. Tang and C. Li, *Mater. Lett.* , 2013, **100**, 15-18.
30. W. Liu, S. He, T. Yang, Y. Feng, G. Qian, J. Xu and S. Miao, *Appl. Surf. Sci.* , 2014, **313**, 498-503.
31. S. Liang, J. Zhou, J. Liu, A. Pan, Y. Tang, T. Chen and G. Fang, *CrystEngComm*, 2013, **15**, 4998-5002.
32. L. Ma, X. Zhou, L. Xu, C. Ye, J. Luo, X. Xu, L. Zhang and W. Chen, *Superlattices Microstruct.* , 2015, **83**, 112-120.
33. W. Wang, L. Li, K. Wu, K. Zhang, J. Jie and Y. Yang, *Appl. Catal. A: Gen.*, 2015, **495**, 8-16.
34. W. Zhang, Y. Wang, D. Zhang, S. Yu, W. Zhu, J. Wang, F. Zheng, S. Wang and J. Wang, *Nanoscale*, 2015, **7**, 10210-10217.
35. P. W. Dunne, A. S. Munn, C. L. Starkey and E. H. Lester, *Chem. Commun.* , 2015, **51**, 4048-4050.
36. E. C. Linganiso, S. D. Mhlanga, N. J. Coville and B. W. Mwakikunga, *J. Alloys Compd.* , 2013, **552**, 345-350.
37. H. Li, H. Li, J. Zhang, W. Dai and M. Qiao, *J. Catal.* , 2007, **246**, 301-307.
38. K. S. Suslick, S. B. Choe, A. A. Cichowlas and M. W. Grinstaff *Nature*, 1991, **353**, 414-416.
39. W. Wang, L. Li, K. Wu, G. Zhu, S. Tan, W. Li and Y. Yang, *RSC Adv.*, 2015, **5**, 61799-61807.
40. R. Akbarzadeh, H. Dehghani and F. Behnoudnia, *Dalton Trans.* , 2014, **43**, 16745-16753.
41. B. Yoosuk, J. H. Kim, C. Song, C. Ngamcharussrivichai and P. Prasassarakich, *Catal. Today* 2008, **130**, 14-23.
42. Q. Liu and J. Zhang, *CrystEngComm*, 2013, **15**, 5087-5092.
43. H. Liu, X. Su, C. Duan, X. Dong and Z. Zhu, *Mater. Lett.* , 2014, **122**, 182-185.
44. H. Zhang, H. Lin, Y. Zheng, Y. Hu and A. MacLennan, *Appl. Catal. B: Environ.*, 2015, **165**, 537-546.
45. Y. Lu, X. Yao, J. Yin, G. Peng, P. Cui and X. Xu, *RSC Adv.*, 2015, **5**, 7938-7943.
46. S.-L. Yang, H.-B. Yao, M.-R. Gao and S.-H. Yu, *CrystEngComm*, 2009, **11**, 1383-1390.
47. K. D. M. Rao, T. Bhuvana, B. Radha, N. Kurra, N. S. Vidhyadhiraja and G. U. Kulkarni, *J. Phys. Chem. C*, 2011, **115**, 10462-10467.
48. K. Zhang, L. Mao, L. L. Zhang, H. S. On Chan, X. S. Zhao and J. Wu, *J. Mater. Chem.* , 2011, **21**, 7302-7307.
49. Y. Song, H. Lee, J. Ko, J. Ryu, M. Kim and D. Sohn, *Bull. Korean Chem. Soc.* , 2014, **35**, 2009-2012.
50. S. Echeandia, P. L. Arias, V. L. Barrio, B. Pawelec and J. L. G. Fierro, *Appl. Catal. B: Environ.*, 2010, **101**, 1-12.
51. C. Bouvier, Y. Romero, F. Richard and S. Brunet, *Green Chem.* , 2011, **13**, 2441-2451.
52. C. Wang, Z. Wu, C. Tang, L. Li and D. Wang, *Catal. Commun.* , 2013, **32**, 76-80.
53. V. M. L. Whiffen and K. J. Smith, *Energy Fuels* 2010, **24**, 4728-4737.
54. E. Furimsky, *Appl. Catal. A: Gen.*, 2000, **199**, 147-190.
55. Y. Yang, H. a. Luo, G. Tong, K. J. Smith and C. T. Tye, *Chin. J. Chem. Eng.* , 2008, **16**, 733-739.
56. Y. Romero, F. Richard and S. Brunet, *Appl. Catal. B: Environ.*, 2010, **98**, 213-223.
57. H. Wan, R. Chaudhari and B. Subramaniam, *Top. Catal.* , 2012 **55**, 129-139.
58. P. Baeza, M. S. Ureta-Zañartu, N. Escalona, J. Ojeda, F. J. Gil-Llambías and B. Delmon, *Appl. Catal. A: Gen.*, 2004, **274**, 303 309.